

Diffusion Tensor Imaging of the Human Optic Nerve Using a Non-CPMG Fast Spin Echo Sequence

Steren Chabert, PhD,^{1,2} Nicolas Molko, MD, PhD,^{1–3} Yann Cointepas, PhD,^{1,2} Patrick Le Roux, MS,⁴ and Denis Le Bihan, MD, PhD^{1,2*}

Purpose: To investigate the diffusion tensor properties of the human optic nerve in vivo using a non-Carr-Purcell-Meiboom-Gill (CPMG) fast spin echo (FSE) sequence.

Materials and Methods: This non-CPMG FSE sequence, which is based on a quadratic phase modulation of the refocusing pulses, allows diffusion measures to be acquired with full signal and without artifacts from geometric distortions due to magnetic field inhomogeneities, which are among the main problems encountered in the orbital area.

Results: Good-quality images were obtained at a resolution of $0.94 \times 0.94 \times 3$ mm. The mean diffusivity (MD) and fractional anisotropy (FA) were respectively $1.1 \pm 0.2 \times 10^{-3}$ mm²/second and 0.49 ± 0.06 , reflecting the optic nerve anisotropy.

Conclusion: This non-CPMG-FSE sequence provides reliable diffusion-weighted images of the human optic nerve. This approach could potentially improve the diagnosis and management of optic nerve diseases or compression, such as optic neuritis, orbit tumors, and muscle hypertrophy.

Key Words: diffusion tensor imaging; optic nerve; non-CPMG fast spin echo sequence; diffusion anisotropy; orbit

J. Magn. Reson. Imaging 2005;22:307–310.

© 2005 Wiley-Liss, Inc.

MRI HAS BEEN WIDELY USED to investigate optic nerve pathology (1). However, conventional MRI techniques suffer from a lack of specificity to the heterogeneous pathological substrates observed in the optic nerve, as well as from a lack of sensitivity to those pathological processes. Diffusion tensor imaging (DTI) represents a promising approach for the study of white matter structures, such as the optic nerve. This noninvasive technique allows the measurement of Brownian motion of water molecules, and thereby provides quan-

titative information on the microstructure of biological tissues (2). The water molecules' displacement is modified by local tissue components. Particularly within white matter, the coherent cell orientation constrains water molecules to move preferentially along the main direction of the neural fibers. This introduces a measurable anisotropy in diffusion that can be quantified (2). Although the origin of the diffusion signal is not yet fully understood, this anisotropy parameter has been shown to be highly sensitive to pathological processes that are typically observed in the optic nerve, such as demyelination and degeneration of white matter tracts, which suggests that it may be useful for assessing diffusion anisotropy within the optic nerve (3,4).

In vitro studies have confirmed the presence of measurable diffusion anisotropy for water diffusion in the optic nerve (5). However, it has always been challenging to image the diffusion properties of the human optic nerve in vivo (6). Indeed, it is a small-sized structure (3–4 mm diameter in the orbital portion (7)) that is prone to motion because it is linked to the freely moving eyeball. The nerve itself is directly surrounded by cerebrospinal fluid (CSF) before it is encircled by orbital fat. Finally, the presence of nearby sinus cavities filled with air and bony structures makes it difficult to image the orbit with conventional echo-planar imaging (EPI) sequences because EPI is sensitive to magnetic susceptibility artifacts (8). Several groups have investigated the diffusivity properties of the optic nerve (4,9,10). All three studies acquired diffusion images only along three directions in order to minimize the acquisition time, whereas a minimum of six diffusion directions is required to fully define the diffusion tensor (DT) (11). The goal of this study was to investigate the diffusion properties of the optic nerve in vivo using DTI. A non-Carr-Purcell-Meiboom-Gill (CPMG) fast spin echo (FSE) sequence was chosen to measure diffusion because this sequence is less prone to susceptibility artifacts compared to EPI sequences (12).

MATERIALS AND METHODS

Non-CPMG FSE Sequence

FSE sequences obey the CPMG condition (i.e., the refocusing pulses are set on an axis perpendicular to the first $\pi/2$ pulse) (13,14). This is necessary to overcome

¹SHFJ/CEA, Orsay, France.

²Federated Research Institute of Functional Neuroimaging (IFR49), Orsay, France.

³INSERM U562, Orsay, France.

⁴General Electric Medical Systems, Buc, France.

*Address reprint requests to: D.L.B., 4 Place du Général Leclerc, 91401 Orsay, France. E-mail: lebihan@shfj.cea.fr

Received June 22, 2004; Accepted April 18, 2005.

DOI 10.1002/jmri.20383

Published online in Wiley InterScience (www.interscience.wiley.com).

the accumulated errors generated by imperfect π pulses that rapidly destroy the transverse magnetization. However, with this scheme the out-of-phase component of the magnetization is destroyed. CPMG-FSE sequences are therefore unable to generate images of complex initial phase, and thus are not well suited to acquire images with diffusion information unless one accepts a reduction of the signal by a factor of 2, in which case the original sequence can be modified (15,16) to be insensitive to the initial phase.

To overcome this problem, Le Roux (12) developed a sequence based on a quadratic phase modulation of the refocusing pulses that allows the system to behave in a stationary manner once it is set in the adequate eigenvector frame. Then, even with nutation angles lower than π , a sustainable train of stable echoes can be acquired that mimics the behavior of classic fast spin echoes, with one component of the echo being constant and the other changing sign every echo. One disadvantage of this non-CPMG FSE sequence is that its echo train length is relatively long compared to that used in EPI. This sequence is thus more sensitive to motion artifacts and T_2 blurring. However, its reduced sensitivity to eddy currents, magnetic field inhomogeneities, and T_2^* blurring makes it very useful for regions of the body where EPI fails on these specific points. The feasibility of diffusion imaging with this non-CPMG FSE sequence has already been shown in both the human brain and the spine, another difficult region (17,18).

Data Acquisition

All images were acquired on a 1.5 T GE Signa Lx scanner (General Electric Medical Systems, Milwaukee, WI, USA). A standard three-inch coil (7.6 cm) was positioned over the volunteer's left eye to collect the signal. T_2 -weighted images and diffusion-weighted images were all acquired using the non-CPMG-FSE sequence.

The study was approved by the local ethics committee. Nine healthy volunteers, who gave written informed consent, participated in this study. Diffusion gradients were applied along six directions:

$$\begin{aligned} & (G_x, G_y, G_z) \\ & = \{(1,0,1), (-1,0,1), (0,1,1), (0,1,-1), (1,1,0), (-1,1,0)\} \end{aligned}$$

using a b-value of 500 seconds/mm². Six repetitions were used, keeping the imaging time relatively short (about five minutes for five slices). The field of view (FOV) was set to 24 × 12 cm and combined with outer volume suppression, giving an in-plane resolution of 0.94 × 0.94 mm. The FSE sequence was used single-shot, and 256 echoes were read with an acquisition bandwidth of 125 kHz. This sequence uses quadratic modulation of the excitation and receiver phases, except for the three first refocusing radiofrequency (RF) pulses, which are devoted to stabilization. The optimization scheme used here is the same as depicted in Ref. 17, with a nutation angle of 160° at the center of the slice. The slice thickness was 3 mm, resulting in a signal-to-noise ratio (SNR) in the diffusion-weighted images of 30:1 (TE = 81 msec). Care was taken to position

the volunteer's head so that the orbital plane containing the optic nerve would be in an axial slice. The slices were positioned carefully so that the nerve would be mostly contained in a single slice. The axial orientation was motivated to maintain identical diffusion and imaging gradients throughout all subjects.

Data Analysis

Regions of interest (ROIs) were placed manually on the T_2 -weighted images by the same investigator throughout the entire study to achieve consistency. All of the computations were done using in-house-written software in C++: *Anatomist* and *BrainVisa* (www.brainvisa.info). The $3 \times 3 \mathbf{b}_i$ matrix was calculated numerically for each of the acquisitions ($i = 1, \dots, 6$) using all the gradient parameters included in the diffusion-weighting portion of the sequence, accounting for the cross-terms, according to Eq. [1] (11)

$$\mathbf{b}_i = \int_0^{TE} \mathbf{k}_i(t) \mathbf{k}_i^T(t) dt \quad (1)$$

with

$$\begin{aligned} \mathbf{k}_i(t) &= \gamma \int_0^t \mathbf{G}_i(t') dt' \quad \text{if } t \leq TE/2 \\ \mathbf{k}_i(t) &= \gamma \int_0^{TE/2} \mathbf{G}_i(t') dt' - \gamma \int_{TE/2}^t \mathbf{G}_i(t') dt' \quad \text{if } t > TE/2 \end{aligned} \quad (2)$$

where γ stands for the gyromagnetic ratio, and the 3×1 vector \mathbf{G}_i is the applied diffusion-encoding gradients on the 3 axis in the i^{th} acquisition. The DT \mathbf{D} was then computed for each pixel according to Eq. [3], where SI_i represents the signal acquired along the i^{th} diffusion direction, SI_0 is the signal acquired with no diffusion weighting, $b_{kl,i}$ is a component of the matrix \mathbf{b}_i , and D_{kl} is a component of \mathbf{D} .

$$SI_i/SI_0 = \exp\left(-\sum_{k=1}^3 \sum_{l=1}^3 b_{kl,i} D_{kl}\right) \quad (3)$$

The mean diffusivity (MD) is equal to one-third of the trace of the DT. We chose to use the fractional anisotropy (FA) index to describe the anisotropy of the nerve. This index is one of the most commonly used invariant indices, and is thus an interesting parameter for comparison. It is defined by a combination of the eigenvalues, λ , of the diagonalized DT (19):

$$FA = \sqrt{\frac{3((\lambda_1 - \langle \lambda \rangle)^2 + (\lambda_2 - \langle \lambda \rangle)^2 + (\lambda_3 - \langle \lambda \rangle)^2)}{2(\lambda_1^2 + \lambda_2^2 + \lambda_3^2)}} \quad (4)$$

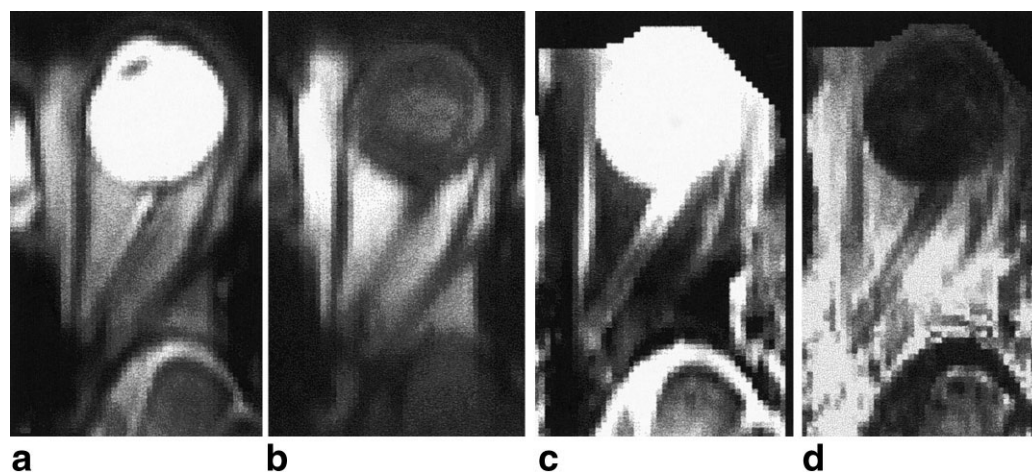


Figure 1. (a) T2-weighted image, (b) diffusion-weighted image along the R/L-S/I direction, (c) MD map, and (d) FA map of the human optic nerve. The nerve is clearly seen surrounded on both sides by CSF on images a, c, and d.

where

$$\langle \lambda \rangle = \frac{\lambda_1 + \lambda_2 + \lambda_3}{3}.$$

Movement was evaluated using SPM99 software (Friston; FIL, London, UK), and the acquisitions were discarded whenever the head moved by more than 2 mm. Using this criterion, two sets of images out of nine were discarded. All data are reported as the mean \pm standard deviation (SD).

RESULTS

The T₂- and diffusion-weighted images, and calculated MD and FA maps of the optic nerve in one representative subject are presented in Fig. 1. The optic nerve is clearly seen surrounded on both sides by CSF on the T₂-weighted images, as well as on MD and FA maps. In the FA map (Fig. 1d) high anisotropy is present in the conjunctive tissue below the eyeball.

The results for each examination are given in Table 1. The mean diffusivities range from 0.8 to 1.3 $\times 10^{-3}$ mm²/second, and FA ranges from 0.39 to 0.56. Averaging over all subjects, the MD in the nerve is 1.1 \pm 0.2 $\times 10^{-3}$ mm²/second, and the FA is 0.49 \pm 0.06.

Table 1
Mean Diffusivity and Fractional Anisotropy in Seven Volunteers

	MD ^{a,b}	FA ^a
Exam 1	1.3 \pm 0.1	0.56 \pm 0.02
Exam 2	1.3 \pm 0.1	0.56 \pm 0.03
Exam 3	1.1 \pm 0.2	0.48 \pm 0.03
Exam 4	1.1 \pm 0.3	0.49 \pm 0.02
Exam 5	1.1 \pm 0.2	0.39 \pm 0.01
Exam 6	1.1 \pm 0.1	0.47 \pm 0.02
Exam 7	0.8 \pm 0.1	0.47 \pm 0.04
Average over exams	1.1 \pm 0.2	0.49 \pm 0.06

^aResults are presented as mean \pm SD in the region of interest.

^b $\times 10^{-3}$ mm²/second.

DISCUSSION

In this study we investigated the diffusion properties of the optic nerve. DT values were obtained using a non-CPMG FSE sequence, which provided good-quality images. The MD found in the optic nerve is consistent with previous reports (4,9,10). To our knowledge, this is the first evaluation in vivo of the DT in the human optic nerve.

Our results differ somewhat from those previously obtained by Iwasawa et al (4) and Freeman et al (9) in the human optic nerve using a spin-echo EPI sequence (cardiac-gated in Iwasawa et al's study). Iwasawa et al (4) measured an apparent diffusion coefficient of 0.98 \pm 0.74 $\times 10^{-3}$ mm²/second along the patient right/left (R/L) direction, and 1.56 \pm 0.74 $\times 10^{-3}$ mm²/second along the superior/inferior (S/I) direction, with a voxel size of 0.625 \times 1.25 \times 3 mm. Freeman et al (9) found it to be equal to 1.21 \pm 0.15 and 1.78 \pm 0.16 $\times 10^{-3}$ mm²/second in the perpendicular and parallel diffusion directions to the nerve, respectively, on voxels of 1.5 \times 1.5 \times 4 mm. Partial volume effects from CSF may have contaminated those results. Iwasawa et al (4) used a low b-value of 262 seconds/mm², which enhances the contribution of fast diffusion compartments, such as CSF-filled spaces. Our results are very similar to those of Wheeler-Kingshot et al (10): with a voxel size of 1.25 \times 1.25 \times 4 mm, the MD was 1.06 \pm 0.10 $\times 10^{-3}$ mm²/second. Since the data from that group were acquired with a CSF suppression technique, it is likely that contamination by the CSF partial volume was slightly higher in our measurements, and contributed to a slight overestimation of our MD results.

Since the orbital fat does not contain any oriented structure (7), we considered the observed anisotropy to be artifactual. The same high anisotropy is also observed in coronal slices, invalidating the hypothesis of contamination by eye motion artifact in the phase-encoding direction (A/P) in the axial slices. Important signal variations were measured from repetition to repetition, which arose from fat in the diffusion-weighted images that was not seen in other parts of the images.

Our understanding is that the signal in the orbital fat area actually comes from a combination of water and fat. Because of the resonance frequency difference between water and fat, the selected fat slice will be misplaced by about 2/9 of the water slice width (i.e., by about 0.7 mm). The combination of diffusion weighting, which significantly decreases the signal only from water, and small movements that modulate the water/fat balance in a given voxel from one image to another, while sensitized to different diffusion directions, produces the signal variations to which FA is known to be highly sensitive, and thus artificially results in false anisotropy. Fat saturation through two 90° RF pulses was implemented, but was not enough to fully suppress signal from the orbital fat. More work must be done to improve fat suppression before this sequence can be used for clinical applications. Since this artifact is restricted to the signal from fat, our measures in the optic nerve should not be contaminated.

This non-CPMG-FSE sequence allows reliable DT images to be obtained in a short time (less than five minutes). Quantitative analysis of diffusivity and anisotropy in the human optic nerve appears to be feasible and has the potential to improve the diagnosis and management of diseases of the optic nerve or orbit, such as optic neuritis, optic nerve compression by tumors, and muscle hypertrophy.

REFERENCES

1. Rizzo 3rd JF, Andreoli CM, Rabinov JD. Use of magnetic resonance imaging to differentiate optic neuritis and nonarteritic anterior ischemic optic neuropathy. *Ophthalmology* 2003;109:1679–1684.
2. Le Bihan D. Looking into the functional architecture of the brain with diffusion MRI. *Nat Rev Neurosci* 2003;4:469–480.
3. Horsfield MA, Jones DK. Applications of diffusion-weighted and diffusion tensor MRI to white matter diseases—a review. *NMR Biomed* 2002;15:570–577.
4. Iwasawa T, Matoba H, Ogi A, et al. Diffusion-weighted imaging of the human optic nerve: a new approach to evaluate optic neuritis in multiple sclerosis. *Magn Reson Med* 1997;38:484–491.
5. Beaulieu C, Allen PS. Determinants of anisotropic water diffusion in nerves. *Magn Reson Med* 1994;31:394.
6. Barker GJ. Diffusion-weighted imaging of the spinal cord and optic nerve. *J Neurol Sci* 2001;186:S45–S49.
7. Miller NR. Walsh and Hoyt's clinical neuro-ophthalmology. Baltimore: Williams and Wilkins; 1982.
8. Mansfield P. Multi-planar image formation using NMR spin echoes. *J Phys C* 1977;10:L55–L58.
9. Freeman AJ, Ballinger R, Werner M, et al. Diffusion weighted EPI of the human optic nerve at 3 T. In: Proceedings of the 6th Annual Meeting of ISMRM, Sydney, Australia, 1998. Abstract 1265.
10. Wheeler-Kingshott D, Parker G, Symms M, et al. ADC mapping of the human optic nerve: increased resolution, coverage and reliability with CSF-suppressed ZOOM-EPI. *Magn Reson Med* 2002;47:24–31.
11. Basser PJ, Mattiello J, Le Bihan D. Estimation of the effective self-diffusion tensor from the NMR spin echo. *J Magn Reson B* 1994;103:247–264.
12. Le Roux P. Non-CPMG fast spin echo with full signal. *J Magn Reson* 2002;155:278–292.
13. Carr HY, Purcell EM. Effects of diffusion on free precession in nuclear magnetic resonance experiments. *Phys Rev* 1954;94:630–638.
14. Meiboom S, Gill D. Modified spin echo method for measuring nuclear relaxation times. *Rev Sci Instrum* 1958;29:668–691.
15. Norris DG, Bornert P, Reese T, Leibfritz D. On the application of ultra-fast RARE experiments. *Magn Reson Med* 1992;27:142–164.
16. Alsop DC. Phase insensitive preparation of single-shot RARE: application to diffusion imaging in humans. *Magn Reson Med* 1997;38:527–533.
17. Bastin ME, Le Roux P. On the application of a non-CPMG single-shot fast spin-echo sequence to diffusion tensor MRI of the human brain. *Magn Reson Med* 2002;48:6–14.
18. Le Roux P, Darquie A, Carlier PG, Clark CA. Feasibility study of non Carr Purcell Meiboom Gill single shot fast spin echo in spinal cord diffusion imaging. *MAGMA* 2002;14:243–247.
19. Basser PJ, Pierpaoli C. Microstructural and physiological features of tissues elucidated by quantitative-diffusion-tensor MRI. *J Magn Reson B* 1996;111:209–219.